Heliyon 10 (2024) e26069

Contents lists available at ScienceDirect

Heliyon

journal homepage: www.cell.com/heliyon

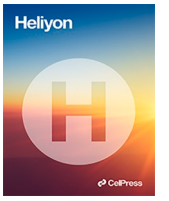

Research article

A fully textile-based, tunable, force and strain sensing resistor for e-textile applications

Adrian K. Stavrakis *, Mitar Simić, Mirjana Damnjanović, Goran M. Stojanović

Faculty of Technical Sciences, University of Novi Sad, Trg. Dositeja Obradovica 6, 21000 Novi Sad, Serbia

ARTICLE INFO

Keywords:
Textile sensor
Smart textiles
Embroidery
Tension testing
Embroidered FSR

ABSTRACT

This work presents a novel approach towards integrating electronic components with textiles, by successfully creating a fully textile-based element that is capable of detecting applied forces by variation in its resistance value. The fabrication of the device consists of a specialized siliconized conductive fabric, which is placed above and below a layer of switch fabric, which acts as a force sensor. In this paper, the effects of three different geometries are observed, as well as the washability of the device, along with tension testing. Moreover, the device behavior is simulated as well as applied in a real-life scenario. The proposed element demonstrates a good dynamic range, high repeatability and stability, and minimal impact of washing, creating a great candidate for integration in e-textiles.

1. Introduction

In recent years, there is a global scientific interest in the migration from conventional electronics to their miniaturized counterparts, which are often flexible or made from unconventional materials, using non-standard lithographic or micro-electromechanical systems (MEMS) fabrication techniques. To that end, a sector of increasing importance, not only in terms of scientific advancements but also of commercial interest, is that of textile electronics, or also commonly termed as e-textiles. Coupled with the recent advancements of wearable devices, many promising applications exist including biomedicine, industry 4.0 and education [1–3]. The primary fabrication methods in the field consist of utilizing conductive threads, thin enameled wires, screen printing of conductive pastes on textile, and hybrid approaches. However, even though primary electronic components such as resistors and capacitors have been successfully migrated by various research groups, the migration of more advanced components is still a work in progress. Some studies include textile electromagnetic induction sensors [4], temperature [5,6], and strain gauge sensors [7,8].

Another component of increasing utilization is the force sensitive resistor (FSR). It is usually fabricated by screen printing of conductive elements on a flexible substrate, and as the name suggests, it works by incrementing or decrementing its nominal resistance with respect to applied compressive force. Some of its most common applications are that of coating screens to enable tactile functionality, replacing on/off switches, gait [9] and sports monitoring [10], monitoring of composite textile structures [11], and generally applications where space is limited, given the very thin profile of FSRs versus mechanical switches. A force sensor is a device that electrically responds to changes in applying force, by varying one of its internal characteristics, most commonly its capacitance or its resistance (passive sensors). In the current state of the art, even though numerous attempts have been made towards creating FSRs using various techniques such as conductive electrodes separated by sheets that form the resisting part [12], conductive bus-coated

* Corresponding author.
E-mail address: sadrian@uns.ac.rs (A.K. Stavrakis).

https://doi.org/10.1016/j.heliyon.2024.e26069
Received 7 July 2023; Received in revised form 6 February 2024; Accepted 7 February 2024
Available online 17 February 2024

regular fabric with eTextile in between [13], etching of Sn–Ag–Cu plated Nylon in Ref. [14] and optical fiber integration [15], there are not many research examples towards fully textile-based fabrication without specialized steps.

Thus, in the current work, a fully textile-based approach is presented to create an FSR and characterize it in terms of electrical performance, stress testing and washability, as well as two variations in the internal geometry were studied, to establish whether these changes can aid in the tunability of the sensor. The novelty of the proposed work can be summarized as following: (a) for the first time we fabricated fully textile-based force sensing resistors, (b) it is a highly cost-effective process without the need for specialist equipment or dedicated fabrication facilities and (c) it utilizes entirely skin-friendly materials, reducing the potential discomfort of the user to minimum.

2. Materials and methods

2.1. The resistive force sensor operating principle

A force sensor is a device that responds to changes in applying force, by varying one of its internal characteristics, most commonly its capacitance or its resistance. This change can be either linear or not, but generally for sensing purposes, linearity is a highly sought after trait. In the case of this paper, the proposed device utilizes the resistive principle. Under which, electrons flow between two non-ideal conductors via a resistive material, and the higher the conductivity exhibited, the less restricted the flow is, hence the lower the resistance.

The total resistance of the sensor, however, is the sum of both the resistance of the material, and the contact resistance at each point of interfacing. In conventional FSRs, this interface is found between the electrodes and the polymer base of the sensor. In textiles, on the other hand, this is a much more complex procedure, as the interfaces cannot be assumed as flat, given the knitted or weaved nature of the fabrics. Therefore, it is beneficial to study this part in depth, as the contact resistance which occurs constantly, is prone to change under three distinct states. The Sharvin contact state, when the device is relaxed, a transitional state when external force starts to act on it, and the Holm contact state, when the device is sufficiently compressed [16].

In the Sharvin state, the flow of the electrical currents is considered to happen through a limited number of contact spots, due to the roughness of the materials at the interface. Occasionally, the mean radius of the contact spots a, may be smaller than the mean electron free path λ, in which case the electrons travel ballistically from one end of the contact to the other, and the Sharvin contact resistance (1) can be found as:

$$R_s = \frac{\lambda(p_1 + p_2)}{2\alpha} \tag{1}$$

with p_1, p_2 denoting the specific resistivity of the two surface ends in contact [17,18].

In the Holm state, it is considered that the two materials at the interface have compressed enough, so that the actual contact can now be approximated by a small circular area for each contact point. Given that each individual contact area is small compared to the entire area physically touching, the small area of current flow between the two materials is called an a-spot, with the "a-" coming from asperity. It can be deduced that for a homogeneous material, its resistivity is also homogeneous, so the current and voltage in the case of an a-spot exhibits circular symmetry, and its size can be associated with the resistance of the electrical contact interface.

Now that the most prominent phenomena that govern the electrical contact interfacing are known, one should again revisit the operating principle at a device level. Under the effect of a given applied force or stress, an elastic deformation occurs at the interface of the sensor layers, and by compressing the materials together, the deformation creates gradually more and flatter contact points. When this occurs, the effective contact area of the sensor layers increases and owing to the states described above, the sensor starts responding with a change in resistance [19].

Here, there are two main operating principles to be found. Quantum tunnelling and percolation. Both of them occur at the same time, however the prevalence is governed by the particle concentration [20]. Even though to date, there is no model or analytical expression that can predict simultaneously any potential non-linearity that can exist in the sensor, these two operating principles define the operation mode of the sensor. Percolation prevails when the particle concentration is above a percolation threshold termed φ_c, and the sensor increments its resistance value as a response to an increment in the applied pressure, hence exhibiting a positive pressure coefficient. In this case, the electrical resistivity ρ can be given for a given stress value σ as seen in Ref. [21] using (2):

$$\rho = \rho_0(\varphi - \varphi_c)^{-x} \tag{2}$$

with x being the critical conductivity exponent, φ being the volume fraction of the material, φ_c the percolation threshold, and ρ_0 being a prefactor stemming from the material transport properties.

On the other hand, in quantum tunnelling operation, an FSR exhibits a negative pressure coefficient, decrementing its resistance for an incrementing value of stress. The general underlying principle is that owing to the exhibited elastic deformation, there is a decrease in the average inter-particle separation, which in turn increases the probability of their transmission. Even though an in-depth analytical description of this would be beyond the scope of the current work, it has been extensively showcased in Ref. [22]. Quantum tunnelling operation is the principle behind the vast majority of the commercial FSR products in circulation and is also the case of the sensor presented in this work. A notable remark on the phenomenon should also be made, as it is also known as hopping in the literature, and another way that it can be measured is by measuring the conductivity of the material or device as a function of temperature. Where hopping conduction would be subject to an increase with higher temperature, ohmic conduction which would reduce with it.

2.2. Sensor design and fabrication

Given its nature, an FSR sensor, is inherently thin, ranging up to 1–2 mm, when constructed using the thin film polymer screen printing technique. Similarly, it should be of adequate surface area to conform to the pressure or force exerting point, usually an actuator or a human finger. Therefore, with these design limitations under consideration, we decided to arbitrarily choose a square geometry of 3 × 3 cm. This includes a necessary seam allowance for the sensor assembly, giving a workable area of 2.5 × 2.5 cm, which is sufficient to accommodate the finger of an adult. The sensor consists of three layers. Two alternate combinations of the central layer were also tested, and in total five samples per geometry were created.

The top and bottom layers are made of a siliconized conductive fabric, Silitex (Shieldex, Bremen, Germany) which according to the manufacturer composition "is a pure silver metallized knitted fabric consisting of 78% polyamide and 22% elastane [23]. The elastane is knitted in warp and weft direction, so that this electrically and thermally conductive textile is stretchable on both sides". It also exhibits a surface resistivity of less than 5 Ω per running meter and a thickness of 0.65 mm.

The middle layer was made from a specialized Knitted Spacer Fabric (Shieldex, Bremen, Germany) which consists of two independent conductive layers only connected by an isolated pile yarn, has a thickness of 3.2 mm and an electrical surface resistivity of less than 5 Ω/m. This unique combination gives it the necessary force sensitive properties, as when released the bottom and top layers are electrically isolated, while when compressed, electron flow starts and the material gradually conducts.

On the first geometry tested, the middle layer was made entirely out of the spacer fabric, while in the second geometry alternating strips of 0.5 cm and generic felt fabric were created, and in the third alternating strips of 0.5 cm and air gap were created. Fig. 1a–c shows the pseudo-3D view of the constructed sensors. In order to bring the sensors together, it was necessary to affix the layers by embroidery, however that posed another problem for consideration. If the embroidery needle was to be driven directly through the spacer fabric, owing to its tension, it would permanently compress it. Therefore, the device was assembled by temporarily affixing the fabric pieces in place using temporary fabric glue, and then an enforced seam was created, in the form of a double center-split seam of 3 mm, using a polyester non-conductive thread. The assembled device can be seen on Fig. 1d.

The embroidery was performed on an industrial embroidery machine (JCZA 0109-550, ZSK, Krefeld, Germany), with a reduced needle tension of 50 g-force (gF) and a standard bobbin thread tension of 22 gF. As that was the minimum allowable tension to form a stitch lock across all layers, but still induced tension to the sensor, a ring of EVA foam was placed directly below the stitching in between the two Silitex layers, to mitigate that. The stitch digitization was realized on the proprietary software of the machine, by importing a vector file of the needed design in Drawing Interchange Format (.dxf). It is worth mentioning that given the conductive nature of the siliconized Silitex fabric, there is no need for interfacing using wiring or other means as leads, as according to the application the sensor can be affixed with various ways to the onward electronics, such as by direct embroidery, by conductive epoxy, press-fit connectors, *etc*. For testing purposes, the instrument leads were directly clamped to it using crocodile clips.

2.3. Resistance testing setup

In order to assess the behavior of the fabricated sensors, the impedance was measured using a portable LCZ meter (U1733C, Keysight, USA), running in parallel with physically mounting the sensor in a tension testing column (34SC-2, Instron, USA) in order to exert the necessary compressive loads. To achieve an as uniform as possible force across the sensor surface area, custom faceplates were created for the tension machine, and printed in Acrylonitrile Butadiene Styrene (ABS) with 100% infill using a fused deposition modelling 3D printer (Ultimaker 2+, Ultimaker, Utrecht, the Netherlands). The faceplates were printed fully-filled, to ensure that they will not compress or deform in the range of operation of the sensor under test. One set of flat and one set of curved faceplates were created. The complete test environment is shown in Fig. 2.

A second role of the custom faceplates is to ensure that any conductive path between the device under test-portable LCZ meter and the tension testing system is disrupted, in order to not invalidate the measurements, given that both systems were running concurrently.

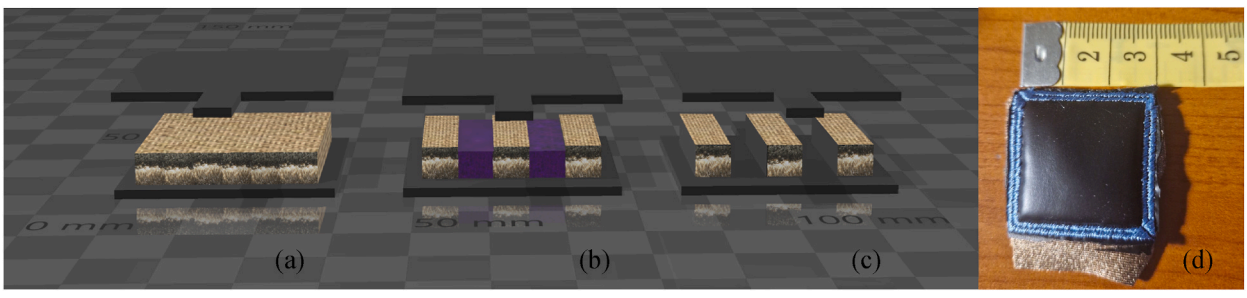

Fig. 1. Exploded view of the proposed sensor, with a solid resistive layer (a), alternating strips of felt and spacer fabric (b) and alternating strips of spacer fabric and air (c), as well as the fabricated device (d). A 3D model file can be found as supplementary material.

Fig. 2. The test setup with the device under test loaded onto the tension testing system and attached to a portable LCZ meter.

2.4. Washability testing

A washability test was designed, in order to assess the performance of the proposed FSR when integrated in a garment that would potentially see general household washing throughout its working lifetime. Even though ideally more cycles would give a clearer picture of the degradation, it was decided to conduct 10 washing and drying cycles to avoid resource wastage, such as water and energy (on average 50 l and 0.78 kWh per cycle) as our preliminary results were not showing such a significant degradation that would mandate the continuation of the washability study until the breakdown of the device. The test was carried out in accordance with the ISO 6330:2021 standard with a washing procedure in a Type A washing machine, where the samples and sufficient ballast to form a 2 kg load were inserted, and 20 g of reference detergent 2 were used, at a temperature of 30 °C, followed by a drying procedure A (Air drying) for each cycle. However, the local water contains 255 ppm of $CaCO_3$ which deviates from the standard requirements of up to 20 ppm [24]. After each test cycle, a measurement was taken across all samples, at unloaded conditions, and in loading of 5 N increments until no more change in the resistance due to compression was observed, followed by unloading in 5 N increments. Even though such compression cycles could arguably affect the washability effects, in reality, the forces experienced by the device inside the machine drum during a wash cycle are several orders of magnitude higher, so as to render the former negligible.

2.5. Cyclic load testing

Lastly, a cyclic load testing was performed across all samples, where the sensor was compressed to 90 % of the maximum compression applied in 2.3, and then decompressed. This was carried out on one sample of each geometry, for 50 repetitions. The aim was to assess any physical damages or morphological deviations to the sensor, as well as to observe the necessary time between decompression and response from the sensor. The same testing environment from section 2.3 was also utilized in this stage.

3. Results and discussion

3.1. Sensor simulation

As a reference point between the expected sensor performance and the real-life measurements, a sensor of similar geometry was simulated in COMSOL Multiphysics, in a multiphysics coupling between electrical currents and solid mechanics. The following two assumptions were made, in order to simplify the simulation and save precious processing time. Firstly, that the fabric materials used are homogenous, *i.e.,* that their density, doping, and weaving are not varying with geometry on any axis. Secondly, the rough contact points described in section 2.1 are approximated as tips of triangles forming the contact between the layers, which, when compressed

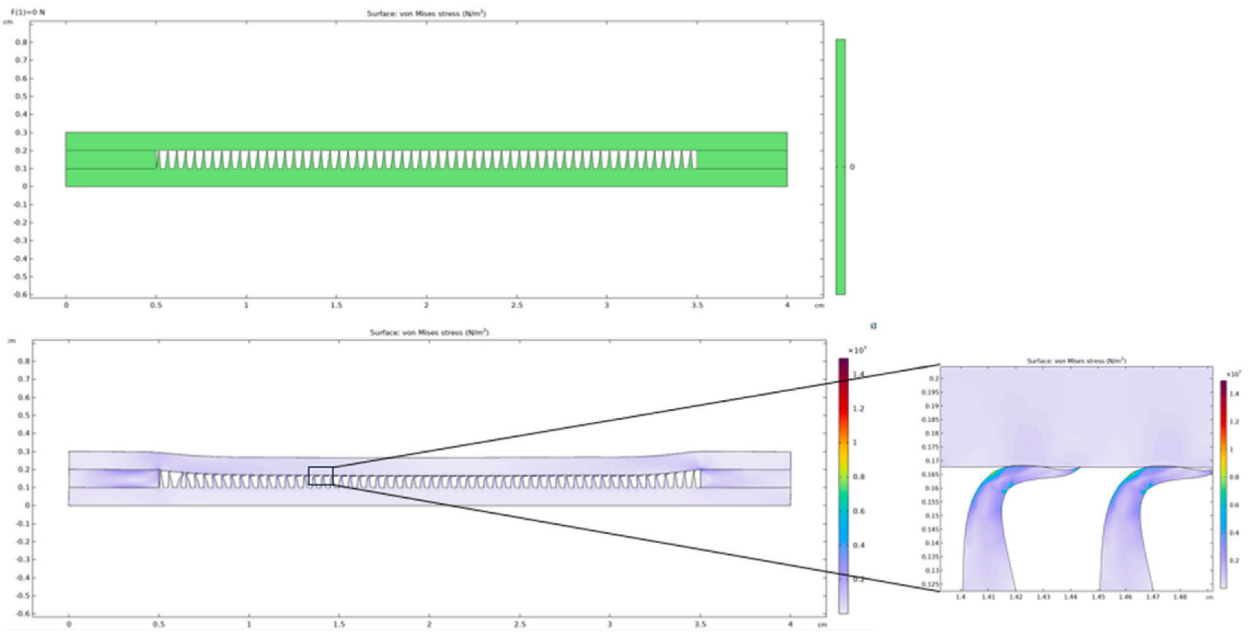

Fig. 3. Initial and compressed states of the force sensing resistor. It can be seen how the material buckles and increases the contact surface area.

enough tilt and create more surface area, thus reducing the resistance of the sensor. An animation of this behavior can be found in the digital supplementary files of the journal, while in Fig. 3, the starting condition and effects of compression on the geometry can be seen, with a zoomed outset for clarity.

3.2. Baseline sensor performance

Initially, a resistance measurement was carried out on all samples in unloaded conditions. As expected, the marking was above the maximum level of the LCZ meter, meaning that the resistance was more than 10 MΩ, classifying the FSR in this stage as a perfect insulator. Then, a compressive force was applied on the samples, until there was no more change in their resistivity. Ten samples of each internal geometry variation as shown in Fig. 1 were used in the testing, during which for each of them a resistance measurement was taken at every 0.25 mm of realized displacement (compression). This allowed for the establishment of the limits of the detection of the sensor. Fig. 4 shows the mean resistance vs. displacement (compression) of each sensor geometry, along with the standard deviation.

As it can be seen, all sensor geometries do exhibit a flattening resistance region at a comparable level of compression, which as expected, is the lowest for the case of only spacer fabric and highest for the case of air interruptions. The increased standard deviation in the latter case, can be attributed to the fact that the initial spacing of the spacer fabric strips is only ensured by a temporary garment adhesive, and not by another material such as felt. Therefore, a reasonable assumption is that across different samples, maybe there were some internal shifts in the strips of the fabric.

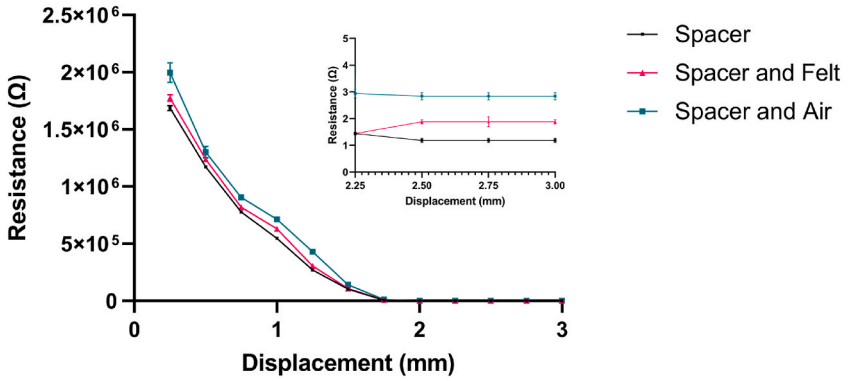

Fig. 4. Mean resistance change and standard deviation per geometry variation vs. displacement. In the inset the linear region has been zoomed in for clarity.

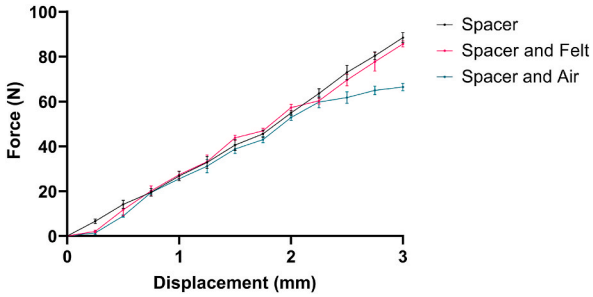

Fig. 5. Changes in force vs. compression by geometry variation.

Similarly, Fig. 5 shows the mean force vs. displacement of each sensor geometry along with the standard deviation, with force measurements taken at the same conditions as the previous step. It can be seen that towards the final levels of compression that result in a resistance change as established in Fig. 4, in general the geometry with air gaps registers less force, followed by the geometry of the spacer fabric only, and trailed by the geometry with felt and spacer fabric strips. This result is very important, as even though it can be explained by the way the test runs, it verifies a very interesting property of the sensors. As the test uses the displacement (in this case compression) as an independent variable, the tension equipment is programmed to only accurately modify this and monitor for changes in force by the force actuator. The reverse would be programmed to stop at fixed force intervals, and monitoring for displacement level changes.

Thus, the clear difference in force registration, particularly in the cases of full fabrics, verifies the tunability of the proposed design. As felt is generally stiffer and more densely woven than the spacer fabric, it shows that by varying the ratio between the fabrics, a stiffer or softer sensor can be achieved, and therefore at any point of its compression it can require less or more force to actuate.

Therefore, from this step of the study, it was verified that a custom combination of spacer fabric, which is primarily responsible for moderating the electron flow between the two conductive fabric layers of the fabric, and a stiffer or softer filler fabric, can modify simultaneously the resistance profile and the force profile of the sensor.

3.3. *Effects of washing*

After observing the behavior of the fabricated sensor variations, a washing test was initiated as described in 2.4 and after every cycle, each sample was compressed and measured before the next. Fig. 6 shows the mean and standard deviation of the measurements at each cycle per variation, at the maximum compression point. It can be observed that in the case of spacer fabric and air, there is a higher variation, both in the standard deviation across the samples at a certain cycle, and in the general trend across the cycles, which can most probably be attributed to the shifting of the spacer fabric pieces inside the device. Therefore, this adverse effect might render this variation not suitable for some applications. However, in the other two cases, the sensors exhibit similar behavior both across the variation of samples at the same wash cycle and across the cycle population.

The similar slope of the two over the consecutive washing cycles, might also be an indicator of a variation in drying conditions, given that they were rack dried in ambient conditions, however that is a known unpredicted effect which can occur at any time. It is interesting that even if that is the case, for example if the cycles 5 and 7 allowed for more drying the performance of the sensor did not significantly change.

3.4. *Cyclic load testing performance*

After observing the effects of washing on the sensor samples, a cyclic load testing was performed as described in section 2.5 by compressing the samples to 2.7 mm, registering the force value, uncompressing them, and repeating this 50 times. Fig. 7 shows the

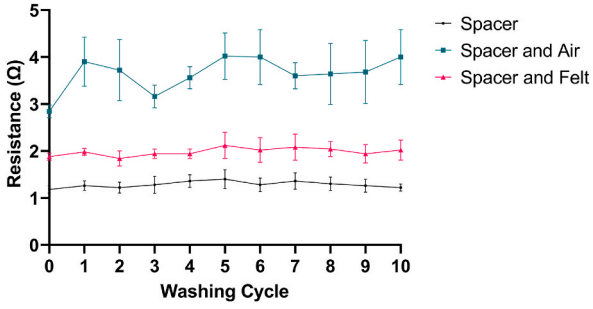

Fig. 6. Mean resistance values and standard deviation of the different sensor geometry variations across washing cycles.

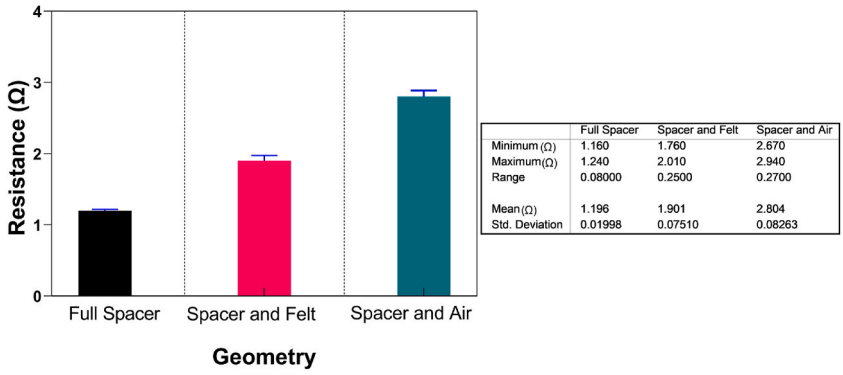

	Full Spacer	Spacer and Felt	Spacer and Air
Minimum (Ω)	1.160	1.760	2.670
Maximum (Ω)	1.240	2.010	2.940
Range	0.08000	0.2500	0.2700
Mean (Ω)	1.196	1.901	2.804
Std. Deviation	0.01998	0.07510	0.08263

Fig. 7. Mean and standard deviation of resistance during cycling load testing, per geometry variation group.

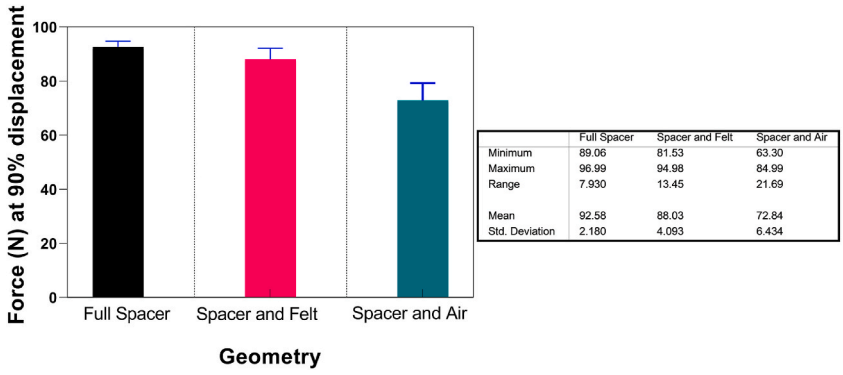

	Full Spacer	Spacer and Felt	Spacer and Air
Minimum	89.06	81.53	63.30
Maximum	96.99	94.98	84.99
Range	7.930	13.45	21.69
Mean	92.58	88.03	72.84
Std. Deviation	2.180	4.093	6.434

Fig. 8. Mean and standard deviation of force during cycling load testing, per geometry variation group.

change of resistance and Fig. 8 the change at force at this point. It can be seen, that with respect to the changes of resistance, that the sensor made entirely from spacer fabric is very stable, with only a mean resistance value of 1.2 Ω and 0.02 standard deviation, while in the case of the sensor from fabric strips and air, the standard deviation quadruples, at 0.08 for a mean resistance of 2.8 Ω.

Similarly, a significantly repetitive behavior can be observed in the case of force at the 90% of maximum compression level, with the most stable variant being that of the spacer fabric, with a standard deviation of only 2.18 around a 92.58 N mean, and the variant with air experiencing a higher deviation of 6.43 around a 72.84 N mean. The generally smaller deviation in the case of spacer and air versus the observed behavior after the washing can be explained by two reasons. Firstly, only one sample out of the five per geometry was loaded for a cyclic test, and secondly, there is a total absence of the mechanical and centrifugal forces experienced during a washing cycle in between the tests.

3.5. *Real application scenario*

Following testing of the individual sensors, we created a 3 × 3 sensor array, in a similar fashion to Fig. 1a, and we embedded this inside a chair pillow. The chair pillow was placed atop a rigid wooden chair (Fig. 9a), and two volunteers were asked to sit upright and still for a period of 60 s. Volunteer A has a BMI of 24.4 kg/m^2 and volunteer B a BMI of 32.5 kg/m^2. The array was connected on one end to the common ground pin of the microcontroller board, and on the other end, the individual values, sampled at 2 samples per second and through Analog-to-Digital conversion, were being wirelessly reported to a mobile phone. A heatmap was then produced per volunteer as seen in Fig. 9b-c.

It can readily be observed that the array is able to detect not only changes in the relative position of the volunteers, but also the extra pressure applied to the chair pillow by volunteer B. Volunteer A has a slightly more balanced posture than volunteer B, and in this case the readings are more equalized. This is a very promising result, since the device can very easily be modified to detect correct seating posture, which is often common among desk users with prolonged use of computers. Additionally, it can detect for how long a user has been sedentary and remind them to take a break. Since already wireless connectivity to a third-party device has been achieved, it is easy to miniaturize the electronics components and switch from a commercial development board to a custom-made solution.

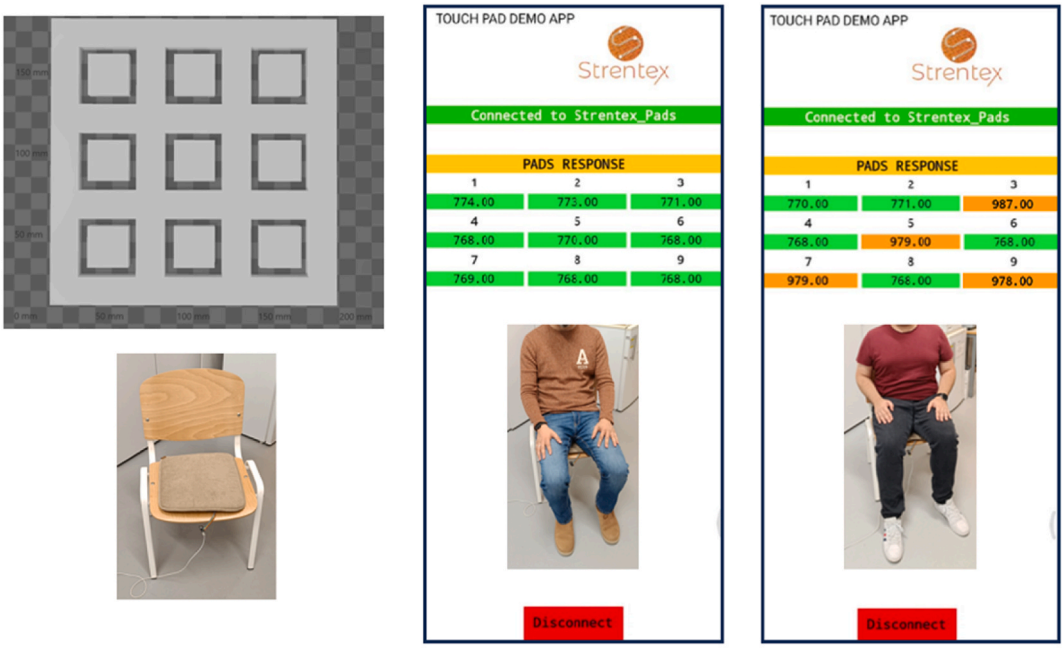

Fig. 9. Render of the sensor array and the embedded setup (a), snapshot of the sensor array response for Volunteer A (b) and Volunteer B (c). The values shown correspond to levels out of the 1023 maximum levels of the onboard ADC of the Arduino board.

4. Conclusions

In this paper the fabrication process of a fully textile-based element was described. This element using the resistive principle, is able to detect changes in applied force by varying its resistance. Three different geometries were studied, as a proof of the tuning capabilities of the proposed sensor, and the findings are indeed validating the claim that by altering the internal geometry different resistance profiles can be achieved that may be suitable for various occasions.

In principle, the advantage of the proposed approach is the fact that by maintaining a standardized external footprint of the device, and by varying the internal conductive layer geometry and materials, the device can be tuned both in terms of the resistance change and in terms of the applied pressure range.

In addition to that, the effects of repeated washing were studied, and the proposed sensor sees an almost complete absence of performance degradation. Lastly, a repeated load cycle of 50 times compressive force loading and releasing showed that the proposed device has a great stability, with deviations of less than 10% across its loading cycles.

Overall, with the proposed material combinations and fabrication methods, we have successfully showcased that a reliable and tunable FSR can be created entirely from textile materials and be directly integrated on garments or be further interconnected with other textile elements. Thus, complemented by our cyclic loading and washability tests, we can reach the argument that the expected lifetime of such a sensor will be comparable to or greater than the textile of the garment surrounding it on potential wearable applications.

5. Future work

In the future, it would be beneficial to the scientific community to test various other structures, in order to best try and tune to the existing resistor values used in conventional electronics, as well as we reserve conducting a more extensive electrical loading test, to also showcase the transient behavior of the created component, bearing in mind the different on-body conditions, such as for example the fact that a conventional ceramic resistor can reach temperatures well above 100 °C before failing, something which is impossible on worn garments in contact or proximity with the skin. Lastly, a friction test might also prove useful in determining whether any fatigue or delamination starts showing on the layer interfaces.

To that end, our group aims to integrate the proposed design in the future in the insoles of shoes in order to provide a platform for assessing gait, walking steadiness and asymmetry, which can cause various problems and their early detection can prevent severe health issues primarily in the elderly. Moreover, we plan to reconstruct the current device with different outer materials, such as for example self-adhesive conductive fabrics, and fabrics of a different level of smoothness, for various scenaria. Lastly, we will aim to develop an integration with bandages, in order to monitor wound healing by assessing and recording in real time the level of swelling

of a wound during its closure.

Funding

This research was funded through the European Union's Horizon 2020 research and innovation programme under grant agreement No. 854194.

Data availability statement

Data presented in this study is available by direct communication with the corresponding author upon reasonable request.

CRediT authorship contribution statement

Adrian K. Stavrakis: Writing – review & editing, Writing – original draft, Visualization, Software, Methodology, Investigation, Formal analysis, Data curation, Conceptualization. **Mitar Simić:** Supervision, Methodology. **Mirjana Damnjanović:** Writing – review & editing, Validation. **Goran M. Stojanović:** Validation, Supervision, Resources, Funding acquisition, Conceptualization.

Declaration of competing interest

The authors declare that they have no known competing financial interests or personal relationships that could have appeared to influence the work reported in this paper.

Appendix A. Supplementary data

Supplementary data to this article can be found online at https://doi.org/10.1016/j.heliyon.2024.e26069.

References

[1] J. Goncalves, L. Leitao, V. Carvalho, Analysis of the reliability and accuracy of a wearable device: Comparative study with a certified clinical device, in: 2017 12th Iberian Conference on Information Systems and Technologies (CISTI), IEEE, Lisbon, Portugal, 2017, pp. 1–6, https://doi.org/10.23919/CISTI.2017.7976034.
[2] A. Mosenia, S. Sur-Kolay, A. Raghunathan, N.K. Jha, Wearable Medical sensor-based system design: a survey, IEEE Trans. Multi-Scale Comp. Syst. 3 (2) (2017) 124–138, https://doi.org/10.1109/TMSCS.2017.2675888.
[3] X. Zhang, C.-W. Wu, P. Fournier-Viger, L.-D. Van, Y.-C. Tseng, Analyzing students' attention in class using wearable devices, in: 2017 IEEE 18th International Symposium on A World of Wireless, Mobile and Multimedia Networks (WoWMoM), IEEE, Jun, Macau, China, 2017, pp. 1–9, https://doi.org/10.1109/WoWMoM.2017.7974306.
[4] D. Teichmann, A. Kuhn, S. Leonhardt, M. Walter, The MAIN shirt: a textile-integrated magnetic induction sensor array, Sensors 14 (1) (2014) 1039–1056, https://doi.org/10.3390/s140101039.
[5] G. Mattana, et al., Woven temperature and humidity sensors on flexible plastic substrates for E-textile applications, IEEE Sensor. J. 13 (10) (2013) 3901–3909, https://doi.org/10.1109/JSEN.2013.2257167.
[6] M. Sibinski, M. Jakubowska, M. Sloma, Flexible temperature sensors on fibers, Sensors 10 (9) (2010) 7934–7946, https://doi.org/10.3390/s100907934.
[7] O. Atalay, W. Kennon, Knitted strain sensors: impact of design parameters on sensing properties, Sensors 14 (3) (2014) 4712–4730, https://doi.org/10.3390/s140304712.
[8] C. Mattmann, F. Clemens, G. Tröster, Sensor for measuring strain in textile, Sensors 8 (6) (2008) 3719–3732, https://doi.org/10.3390/s8063719.
[9] F. Lin, A. Wang, Y. Zhuang, M.R. Tomita, W. Xu, Smart insole: a wearable sensor device for unobtrusive gait monitoring in daily life, IEEE Trans. Ind. Inf. 12 (6) (2016) 2281–2291, https://doi.org/10.1109/TII.2016.2585643.
[10] B. Zhou, M. Sundholm, J. Cheng, H. Cruz, P. Lukowicz, Never skip leg day: a novel wearable approach to monitoring gym leg exercises, in: 2016 IEEE International Conference on Pervasive Computing and Communications (PerCom), IEEE, Mar., Sydney, NSW, 2016, pp. 1–9, https://doi.org/10.1109/PERCOM.2016.7456520.
[11] S. Kursun Bahadır, Identification and modeling of sensing capability of force sensing resistor integrated to E-textile structure, IEEE Sensor. J. 18 (23) (2018) 9770–9780, https://doi.org/10.1109/JSEN.2018.2871396.
[12] M. Sundholm, J. Cheng, B. Zhou, A. Sethi, P. Lukowicz, Smart-mat: recognizing and counting gym exercises with low-cost resistive pressure sensing matrix, in: Proceedings of the 2014 ACM International Joint Conference on Pervasive and Ubiquitous Computing, ACM, Seattle Washington, 2014, pp. 373–382, https://doi.org/10.1145/2632048.2636088.
[13] W. Xu, M.-C. Huang, N. Amini, L. He, M. Sarrafzadeh, eCushion: a textile pressure sensor array design and calibration for sitting posture analysis, IEEE Sensor. J. 13 (10) (2013) 3926–3934, https://doi.org/10.1109/JSEN.2013.2259589.
[14] C. Usma, A.Z. Kouzani, J.J.C. Chua, A. Arogbonlo, S. Adams, I. Gibson, Fabrication of force sensor circuits on wearable conductive textiles, Procedia Technol. 20 (2015) 263–269, https://doi.org/10.1016/j.protcy.2015.07.042.
[15] C.-A. Bunge, et al., Textile multitouch force-sensor array based on circular and non-circular polymer optical fibers, IEEE Sensor. J. 20 (14) (2020) 7548–7555, https://doi.org/10.1109/JSEN.2020.2985328.
[16] A. Mikrajuddin, F.G. Shi, H.K. Kim, K. Okuyama, Size-dependent electrical constriction resistance for contacts of arbitrary size: from Sharvin to Holm limits, Mater. Sci. Semicond. Process. 2 (4) (1999) 321–327, https://doi.org/10.1016/S1369-8001(99)00036-0.
[17] "Resistivity," in Semiconductor Material and Device Characterization, 2005, pp. 1–59, https://doi.org/10.1002/0471749095.ch1.
[18] Contact resistance and Schottky barriers, in: Semiconductor Material and Device Characterization, 2005, pp. 127–184, https://doi.org/10.1002/0471749095.ch3.
[19] L. Paredes-Madrid, C. Palacio, A. Matute, C. Parra Vargas, Underlying physics of conductive polymer composites and force sensing resistors (FSRs) under static loading conditions, Sensors 17 (9) (2017) 2108, https://doi.org/10.3390/s17092108.

[20] S. Stassi, V. Cauda, G. Canavese, C. Pirri, Flexible tactile sensing based on piezoresistive composites: a review, Sensors 14 (3) (2014) 5296–5332, https://doi.org/10.3390/s140305296.
[21] M. Basta, V. Picciarelli, R. Stella, An introduction to percolation, Eur. J. Phys. 15 (3) (1994) 97–101, https://doi.org/10.1088/0143-0807/15/3/001.
[22] J.G. Simmons, Electric tunnel effect between dissimilar electrodes separated by a thin insulating film, J. Appl. Phys. 34 (9) (1963) 2581–2590, https://doi.org/10.1063/1.1729774.
[23] Shieldex, "Silitex Datasheet" Accessed: January. 4, 2022 [Online]. Available: https://www.shieldex.de/en/products/shieldex-silitex/.
[24] Prilog za godisnji izvestj NS Vodovod, Institut za javno zdravlje Vojvodine, Accessed: March. 1, 2023. [Online]. Available: https://www.izjzv.org.rs/uploads/589d4b9c-b827-493b-392d-1445583523a3/2016%20Prilog%20za%20godisnji%20izvestj%20NS%20Vodovod.pdf, 2017.